Sinking CO_2 in supercritical reservoirs

Francesco Parisio[1,†], Victor Vilarrasa[2,3,4*,†]

[1] Chair of Soil Mechanics and Foundation Engineering, Institute of Geotechnics, Technische Universität Bergakademie Freiberg, Germany.

[2] Institute of Environmental Assessment and Water Research (IDAEA), Spanish National Research Council (CSIC), Barcelona, Spain.

[3] Mediterranean Institute for Advanced Studies (IMEDEA), Spanish National Research Council (CSIC), Esporles, Spain.

[4] Associated Unit: Hydrogeology Group UPC-CSIC, Barcelona, Spain.

*Correspondence to: victor.vilarrasa@idaea.csic.es

†The authors contributed equally.

Key points

- We propose a novel geologic carbon storage concept that reduces the buoyancy-driven CO_2 leakage risk.
- By injecting CO_2 in reservoirs where the resident water stays in supercritical conditions, CO_2 sinks because it is denser than pore water.
- Supercritical reservoirs are found at relatively shallow depths between 3 to 5 km in deep volcanic areas.

Abstract

Geologic carbon storage is required for achieving negative CO_2 emissions to deal with the climate crisis. The classical concept of CO_2 storage consists in injecting CO_2 in geological formations at depths greater than 800 m, where CO_2 becomes a dense fluid, minimizing storage volume. Yet, CO_2 has a density lower than the resident brine and tends to float, challenging the widespread deployment of geologic carbon storage. Here, we propose for the first time to store CO_2 in supercritical reservoirs to reduce the buoyancy-driven leakage risk. Supercritical reservoirs are found at drilling-reachable depth in volcanic areas, where high pressure ($p>21.8$ MPa) and temperature ($T>374$ ºC) imply CO_2 is denser than water. We estimate that a CO_2 storage capacity in the range of 50-500 Mt yr^{-1} could be achieved for every 100 injection wells. Carbon storage in supercritical reservoirs is an appealing alternative to the traditional approach.

Plain Language Summary

Geologic carbon storage, which consists in returning carbon deep underground, should be part of the solution to effectively reach carbon neutrality by the mid of the century to mitigate climate change. CO_2 has been traditionally proposed to be stored in sedimentary rock at depths below 800 m, where CO_2 becomes a dense fluid, minimizing the required storage volume. Nevertheless, CO_2 is lighter than brine in the traditional concept, so a rock with sufficient sealing capacity should be present above the storage formation to prevent leakage. Indeed, one of the main hurdles to deploy geologic carbon storage is the risk of CO_2 leakage. To reduce this risk, we propose a novel storage concept that consists in injecting CO_2 in reservoirs where the pore water stays in supercritical conditions (pressure and temperature higher than 21.8 MPa and 374 ºC, respectively) because at these conditions, CO_2 becomes denser than water. Consequently, CO_2 sinks, leading to a safe long-term storage. This concept, which could store a significant portion of the total requirements to decarbonize the economy, should start being implemented in deep volcanic areas, given that supercritical reservoirs are found at relatively shallow depths between 3 to 5 km.

Keywords

1. Introduction

Carbon Capture and Storage (CCS) is envisioned as a key technology to accomplish net negative carbon dioxide (CO_2) emissions during the second half of the century and meet the COP21 Paris Agreement targets on climate change (IPCC, 2018; Bui et al., 2018). However, CCS should overcome two main hurdles, namely the risks of induced seismicity (Zoback & Gorelick, 2012; Vilarrasa & Carrera, 2015) and CO_2 leakage (Lewicki et al., 2007; Nordbotten et al., 2008; Romanak et al., 2012), before its widespread deployment takes place. Proper site characterization, monitoring and pressure management should allow minimizing the risk of perceivable induced seismicity in Gt-scale CO_2 injection (Rutqvist et al., 2016; Celia, 2017; Vilarrasa et al., 2019). The considered storage formations to date include deep saline aquifers, depleted oil and gas fields and unmineable coal seams in which CO_2 stays in supercritical conditions with a relatively high density, but lower than the one of the resident brine (Hitchon et al., 1999). Thus, the risk of CO_2 leakage, although low (Alcalde et al., 2018), may be present for up to millions of years until all CO_2 becomes dissolved into the resident brine or mineralized (Benson & Cole, 2008).

A few concepts have been proposed to date to reduce the risk of CO_2 leakage. These concepts consist either in promoting fast mineralization or storing CO_2 already dissolved in the resident brine. Regarding rapid CO_2 mineralization, injecting CO_2 in shallow basaltic rock allows a quick mineralization thanks to the favorable chemical composition of the host rock, although leakage through buoyancy remains a major concern in the absence of low-permeable caprocks or whenever the caprock integrity is compromised (Gislason & Oelkers, 2014). Another storage rock for mineralization could be peridotite, in which carbonation occurs naturally when exposed to atmospheric CO_2 (Kelemen & Matter, 2008). Peridotite is rare at shallow depths and its total capacity for CO_2 storage is in the order of Gt, provided that the rock is massively hydraulically fractured to reach all the available mineral. Regarding dissolved CO_2 storage, the leakage risk is mitigated because brine is heavier when it is CO_2-saturated (Burton & Bryant, 2009; Sigfusson et al., 2015). CO_2 dissolution can be performed either on surface (Burton & Bryant, 2009) or at the reservoir depth (Pool et al., 2013). To balance the injection and pumping energetic cost, geothermal heat can be recovered and even electricity could be produced if the temperature is high enough (Pool et al., 2013). However, this storage concept has the drawback that CO_2 injection capacity is limited by CO_2 solubility into the brine, which is around 4 % at 60 °C. Such solubility

78   leads to a storage of roughly 0.1 Mt of CO_2 per year and per doublet for a circulating brine flow

79   rate of 80 l s^{-1}, i.e., 2.5 Mt yr^{-1} of water being pumped and re-injected. Thus, very large volumes

80   of brine would need to be circulated – a scenario that makes injection of dissolved CO_2 only

81   feasible for small-scale decentralized CO_2 storage. Overall, the alternatives that have been

82   proposed to reduce the risk of CO_2 leakage entail a limited storage capacity per well with respect

83   to conventional CO_2 injection in free-phase, which diminishes their attractiveness.

84   To overcome this limitation, we propose an innovative CO_2 storage concept that reduces the CO_2

85   leakage risk, does not require the presence and integrity of a caprock and maintains a high storage

86   capacity per well. This concept consists in storing CO_2 in free-phase into supercritical reservoirs,

87   i.e., reservoirs where water is in supercritical state. Supercritical reservoirs are found in the deeper

88   part of volcanic areas (depth > 3 km), where pressure, p, and temperature, T, of the pore water are

89   likely to exceed its critical point ($p > 21.8$ MPa and $T > 374$ ºC for pure water). At water's

90   supercritical conditions, an interesting situation occurs: CO_2 density is higher than the one of water

91   and thus, sinks. Consequently, a low-permeable caprock is not needed in deep volcanic areas.

92   Injecting CO_2 into deeper and hotter reservoirs is a new concept that we propose and we deem

93   possible in the light of the recent achievements in deep drilling in volcanic areas demonstrated at

94   the IDDP-2 project, in which a 4.5 km deep well has been drilled in the Reykjanes volcanic area,

95   Iceland, reaching supercritical water conditions (Friðleifsson et al., 2017).

96   We examine the potential of storing CO_2 in deep volcanic areas where resident water is in

97   supercritical state. First, we analyze the plausible injection conditions at the wellhead that permit

98   injecting CO_2 with a reasonable compression cost. Next, we explore the CO_2 sinking potential and

99   quantify the CO_2 plume shape and injectivity. Finally, we estimate the injection rates that could be

100   achieved and discuss the worldwide CO_2 storage potential in deep volcanic areas.

101   2. Materials and methods

102   2.1. Water and CO_2 equation of state

103 The equation of state (EOS) of water and CO_2 are computed via the C++ library CoolProp (Bell et

104 al., 2014), available at http://www.coolprop.org/. CoolProp employs the Span and Wagner (1996)

105 EOS of CO_2, which is valid up to 800 MPa pressure and 1100 K temperature, and the Scalabrin

106 et al. (2006) viscosity model. The EOS of water is valid up to 1 GPa of pressure and 2000 K

107 temperature and is taken after Wagner and Pruß (2002), which is based on the IAPWS Formulation

108 1995. The viscosity of water is taken after Huber et al. (2009).

2.2. Temperature, pressure and density profiles along the wellbore

110 We have implemented an explicit scheme to compute the fluid properties variation with depth

111 along the wellbore. During CO_2 injection, the cold fluid quenches the well in a relatively short

112 time (days to months), so that at equilibrium a colder annulus forms around the well, hindering

113 heat transfer from the surrounding rock, and the injection process becomes adiabatic (Pruess,

114 2006). The enthalpy is fixed at corresponding wellhead conditions of pressure and temperature

115 $h(z_0) = f(p(z_0), T(z_0))$ and CO_2 density is evaluated with CoolProp functions along the

116 discretized ($n = 1000$ intervals) wellbore depth as a function of temperature and pressure

117 $\rho(z_i) = f(p(z_i), T(z_i))$. At each depth increment $i+1$, the pressure increase is given by

118 $p(z_{i+1}) = p(z_i) + g\rho(z_i)(z_{i+1} - z_i)$, where g is gravity acceleration, and $T(z_{i+1} - z_i)$ is calculated

119 assuming constant enthalpy $h(z_i) = h(z_0)$.

120 To compute the initial reservoir in-situ conditions of the resident water, the weight of the water

121 column to the corresponding depth is calculated assuming thermal equilibrium with the geothermal

122 gradient, hence the only difference with the described procedure is that $T(z_i)$ is known a priori.

2.3. CO_2 plume calculations

124 We use both analytical and numerical solutions to compute CO_2 injectivity (ratio between flow

125 rate and wellhead pressure) and the plume geometry (see SI for more details). For the analytical

126 solution, we use the Dentz and Tartakowsky (2009) solution with the correction to incorporate

127 CO_2 compressibility effects of Vilarrasa et al. (2010). The CO_2 plume evolution is computed for a

128 specific injection scenario of temperature and pressure that is deemed to be representative of the

129 application. We assume initial pore fluid pressure of 34 MPa and temperature of 500 °C and a

130 pressure buildup at the wellhead of 10 MPa in isothermal conditions. The analytical solution is

131 valid for a confined aquifer scenario, which we have assumed to be 500-m or 1000-m thick. The

132 hypothesis of a confined aquifer represents a lower bound case in terms of injection rate: the

133 structural geology features at depth in volcanic areas are quite uncertain and the presence of low-

134 permeability structures could be represented by faults, chemically altered layers or magmatic
135 intrusions, but could not be present as well.

136

3. Results

3.1. Injection conditions in the wellbore

139 CO_2 downhole pressure and temperature conditions are constrained by limiting reservoir cooling
140 and by ensuring an adequate flow rate through sufficient pressure buildup. Assuming wellbore
141 quenching during continuous injection, the injection temperature and pressure at depth depend on
142 the CO_2 wellhead temperature and pressure (Figs. 1 and S1). According to the EOS of CO_2, its
143 density is a function of both temperature and pressure and the adiabatic compression generates an
144 increase in CO_2 temperature with depth (inset in Fig. 1). The density profile, in turn, is responsible
145 for the weight of the fluid column, which translates into a pressure increase with depth (Fig. S1).
146 At 5 MPa of wellhead pressure, the downhole conditions mildly depend on the wellhead
147 temperature. CO_2 is strongly heated up by compression along the wellbore because of its high
148 compressibility as it transitions from gas to supercritical fluid (the critical point of CO_2 is
149 $T = 31.04$ °C and $p = 7.39$ MPa) and reaches the reservoir at approximately 100 °C and $15-17$
150 MPa, a pressure lower than the one of the reservoir that prevents CO_2 flow into the rock. At a
151 wellhead pressure slightly above the critical pressure (see 7.5 MPa in Fig. 1), the downhole
152 conditions strongly depend upon the wellhead temperature because of phase transition phenomena.
153 While CO_2 is in its supercritical phase when injected warmer than its critical temperature, CO_2 is
154 in liquid phase for cooler injection temperature and reaches the reservoir with higher pressure and
155 lower temperature because of the higher density of the liquid than its gas or supercritical phases.
156 A similar situation occurs when the wellhead pressure equals 10 MPa. At 20 MPa of wellhead
157 pressure, the downhole conditions exhibit small changes between wellhead and downhole
158 temperature because CO_2 density changes are small at such high pressure.

159 Downhole overpressure is necessary to ensure that CO_2 enters into and flows within the reservoir
160 and, if we assume a reservoir pore fluid pressure as in IDDP-2 of 34 MPa (Friðleifsson et al.,
161 2017), the downhole pressure should not fall below approximately 40 MPa. For example, to
162 achieve such downhole pressure, the wellhead temperature should not exceed 30 °C for a wellhead

163 pressure of 7.5 MPa. We can limit reservoir cooling only by injecting at high wellhead pressure
164 and temperature, which implies a high energetic cost.

3.2. CO_2 sinking potential

166 Above the critical point of water, both fluids are in supercritical phase and CO_2 becomes denser
167 than water at increasingly higher pressure as temperature increases (Fig. 2). The black solid lines
168 in Fig. 2 indicate the pressure and temperature conditions reached by a hydrostatic water column
169 at several depths by taking into account a range of geothermal gradients typical of volcanic areas,
170 indicated with dotted lines. Fig. 2 also shows the CO_2 injection conditions for a wellhead pressure
171 of 10 MPa and several wellhead temperatures along with the estimated in situ conditions of IDDP-
172 2 of 34 MPa and 500 °C (Friðleifsson et al., 2017). For a wellhead pressure of 10 MPa, the
173 maximum wellhead temperature to enable CO_2 injection is approximately 40 °C. At higher
174 wellhead temperature, the CO_2 density along the wellbore is too small to yield a downhole pressure
175 higher than the one of the reservoir. Thermal exchange heats up CO_2 as it flows through the
176 reservoir and CO_2 temperature and pressure equilibrate to the ones of the reservoir at a given
177 distance from the injection point. The starting and end points of the path (yellow line in Fig. 2) in
178 the phase diagram depend upon the reservoir initial conditions and the wellhead injection pressure
179 and temperature. Following our assumptions, the optimum in terms of CO_2 sinking potential
180 corresponds to gradients between 90 and 120 $K\,km^{-1}$ and at depths > 5 km.

3.3. CO_2 plume and injectivity

182 The analytical solution of Dentz and Tartakowsky (2009), with the correction of Vilarrasa et al.
183 (2010) applied to consider CO_2 compressibility effects for accurately computing CO_2 density
184 within the plume, estimates a downward CO_2 plume (Fig. 3a). We consider a 10-year injection of
185 CO_2 over 500 m and 1000 m-thick reservoirs, assuming a pressure buildup of 10 MPa in a water-
186 saturated reservoir initially at $p = 34$ MPa and $T = 500$ °C. The extension and shape of the plume
187 are a function of the reservoir permeability and thickness, with its maximum located in the lower
188 part of the reservoir. The maximum extension of the downward plume spans over almost 2 orders
189 of magnitude for a range of permeability of 3 orders of magnitude, ranging from approximately
190 2.5×10^2 m for the least permeable case, to approximately 1.0×10^4 m for the most permeable one.
191 The achievable mass flow rate is also proportional to the reservoir permeability and thickness and

192 ranges from 0.0057 Mt yr^{-1} to 4.4 Mt yr^{-1} for a 500 m-thick reservoir, and from 0.012 Mt yr^{-1}

193 to 8.7 Mt yr^{-1} for a 1000 m-thick reservoir.

194 The gravity number N (Eq. (S5)), which is the ratio between gravity to viscous forces, is computed

195 for the near field ($T = 50$ °C and $p = 44$ MPa), i.e., close to the injection point, and for the far

196 field ($T = 500$ °C and $p = 34$ MPa), i.e., the initial reservoir conditions. At the near field, water is

197 liquid with $\rho_w = 1006.3\,\text{kg m}^{-3}$ and CO_2 is supercritical with $\rho_c = 940.2\,\text{kg m}^{-3}$, which yields a

198 $|\Delta\rho| = 66.2\,\text{kg m}^{-3}$ that favors CO_2 buoyancy. At the far field, both fluids are supercritical, with

199 $\rho_w = 138.1\,\text{kg m}^{-3}$ and $\rho_c = 219.2\,\text{kg m}^{-3}$, which yields a $|\Delta\rho| = 81.0\,\text{kg m}^{-3}$ that favors CO_2 sinking.

200 For a 500 m-thick reservoir, the gravity number is $N = 8.389 \times 10^{-1} \approx 1$ for the near field and

201 $N = 2.715 \times 10^3 >> 1$ for the far field, and for a 1000 m-thick reservoir, $N = 1.678 \times 10^0 \approx 1$ for

202 the near field and $N = 5.430 \times 10^3 >> 1$ for the far field conditions. According to the gravity

203 number values, at the near wellbore range, viscous forces dominate or are in the range of gravity

204 forces and far enough from the injection point, buoyant forces become predominant. Although the

205 near field conditions would favor CO_2 buoyancy, viscous forces are in the same range of buoyant

206 ones and thus, CO_2 buoyancy does not take place or is limited in very thick reservoirs. Far from

207 the injection well, buoyant forces dominate over viscous forces, and since CO_2 has a higher density

208 than water, CO_2 tends to sink (Fig. 4). Finite element analyses of CO_2 injection further confirm

209 that an uprising CO_2 plume does not develop near the injection well and that CO_2 sinks once it

210 reaches thermal equilibrium with the rock (Fig. 3b and Fig. 4). The cooled region concentrates

211 around the injection well (Fig. 3b) and even though CO_2 is lighter than water within this cold

212 region, no upward flow occurs due to buoyancy. Thus, CO_2 sinks, leading to a safe storage despite

213 cooling around the injection well.

4. Discussion

4.1. Challenges

216 The coupling between the wellbore and the reservoir is important in storage formations with high

217 temperature, like deep volcanic areas. The conflicting objectives of limiting cooling to minimize

218 the risk of inducing seismicity in the long term (Parisio et al., 2019a) and of minimizing

219 compression costs by lowering wellhead pressure can only be resolved with accurate optimization

220 procedures. Since CO_2 density decreases with temperature, the lower the injection temperature,

221 the higher the downhole injection pressure (Fig. 2). Thus, a trade-off arises between the injection

222 pressure and temperature at the wellhead. The optimum injection conditions are site specific and

223 should be computed according to the characteristics of each site. The pressure and temperature

224 injection conditions at the wellhead are coupled to the injectivity of the reservoir and thus, to the

225 required pressure buildup at the downhole to inject a given mass flow rate. Given the highly non-

226 linearity of flow along a wellbore (Lu & Connell, 2014), the wellhead injection conditions will be

227 determined by the injection mass flow rate and the reservoir transmissivity.

228 Injecting relatively cold CO_2 ($T = 20$ °C) reduces the compression costs because of its higher

229 density (Fig. 2). The most energetically efficient option is to inject CO_2 in liquid state, i.e.,

230 $T < 31.04$ °C (Vilarrasa et al., 2013), a solution that bears the consequence of cooling down the

231 rock in the vicinity of the injection well. Cooling-induced thermal stress is inversely proportional

232 to the injection temperature and is likely to enhance injectivity (Yoshioka et al., 2019), but also

233 microseismicity by approaching failure conditions: operators may therefore prefer to inject CO_2 at

234 a relatively high temperature ($40 \div 60$ °C). Heating CO_2 entails large energetic costs (Goodarzi et

235 al., 2015), which in volcanic areas could be minimized by extracting heat from existing geothermal

236 wells. Injecting hot also increases compression cost because the higher the injection temperature,

237 the higher the required wellhead injection pressure. The energy spent to compress the CO_2 should

238 have a renewable source to comply with the objective of reducing CO_2 emissions. Unlike solar or

239 wind resources, which provide time-fluctuating power output, geothermal energy best fits the

240 purpose of providing a time-constant heat supply required for continuous CO_2 injection.

241 Combining geothermal energy production with geologic carbon storage is of particular interest to

242 utilize the injected CO_2 and generate a synergy to maximize the cut of CO_2 emissions in volcanic

243 areas. Exploiting a volcanic area for both geothermal and CO_2 storage purposes would foster

244 subsurface characterization, reducing uncertainty and identifying the most suitable areas for both

245 geothermal production and geologic carbon storage. CO_2 could be eventually used as working

246 fluid once the CO_2 plume has grown enough (Randolph & Saar, 2011).

247 **4.2.Managing risks**

248 The CO_2 injection rates in deep volcanic areas can be of up to several Mt per year per well (Fig.

249 3a). High injection rates induce pressure buildup and cooling that will in turn affect the

250 geomechanical stability of faults and potentially induce seismic events. Pressure buildup is the

251 main triggering mechanism in the short term and cooling dominates in the long term. The latter

252 may limit the lifetime of injection projects if induced earthquakes become too frequent or of

253 excessively high magnitude (Parisio et al., 2019a). The thresholds in frequency and magnitude of

254 induced seismicity is site specific, and depends on the local structural and tectonic features.

255 Thresholds to induced seismicity, both in terms of magnitude and frequency, depend on the local

256 conditions and on the consequences produced on the population and infrastructure: the risk might

257 be low in isolated areas, but unbearably high in densely populated volcanic areas around the world.

258 In any case, induced seismicity risks should be minimized through subsurface characterization,

259 continuous monitoring and adequate pressure and temperature management.

260 The risks of CO_2 injection in volcanic areas are site-specific, should be carefully assessed and

261 evaluated prior to each potential development project. These risks are connected with the intrinsic

262 risks of active volcanism, namely, CO_2 degassing, hydrothermal explosions and magmatic

263 eruptions – occurrences that could raise concerns about the feasibility of anthropogenic CO_2

264 injection. CO_2 degassing is naturally present in volcanic areas and usually has its origin at boiling

265 aquifers with superheated steam, which is buoyant (Chiodini et al., 2001). For the injected CO_2 to

266 leak and eventually reach the surface, it should reverse its sinking tendency and become buoyant.

267 However, our proposal only considers injecting CO_2 in supercritical reservoirs, which are placed

268 much deeper and at higher temperature and pressure than boiling aquifers. Yet, similarly to what

269 happens in magma chambers, the denser fluid, i.e., CO_2, might migrate laterally outside of the

270 storage formation and encounter different temperature and pressure conditions at which CO_2

271 becomes buoyant (Gudmundsson, 2020). Hydrothermal explosions are caused by spinodal

272 decomposition from metastable states leading to fast re-equilibration phenomena (Thiery &

273 Mercury, 2009) and the relative risks can be increased by long-term fluid extraction in geothermal

274 reservoir, where the pressure drop could bring the system closer to metastable states. We argue

275 that injecting CO_2 will prevent excessive pressure drawdowns and will help maintain a safe

276 distance in the fluid phase-space from metastable and dangerous states, where explosive fluid

277 demixing is possible. The risks of magmatic eruptions are strongly linked with the volcanic activity

278 of a specific site. Consequently, volcanic centers with recent eruptive manifestation should be

279 avoided as target areas of deep CO_2 injection. Avoiding recently active volcanic centers is seldom

280 restrictive in terms of geographical development because supercritical resident brine can be

281 potentially found at drillable depth in several parts of the world where volcanic manifestations are
282 present (Elders et al., 2014). As an example, the Acoculco Caldera Complex has shown no sign of
283 volcanic activity in the form of eruptions and lava flows since approximately 60,000 years ago
284 (Sosa-Ceballos et al., 2018). Nonetheless, two wells drilled within the Caldera recorded a very
285 high geothermal gradient, with approximately 300 ℃ at 2 km depth (Calcagno et al., 2018).

286 The feasibility of this technology is strictly connected to the drilling technology available and to
287 the possibility of reaching pressure and temperature above the critical point of water such that CO_2
288 would sink. For geothermal gradients of 30 K km^{-1}, the critical point of water would be
289 encountered at around 13 km depth, which is currently beyond the available drilling technology.
290 In volcanic areas, because of the higher geothermal gradients, the critical point of water is located
291 at the accessible depth of 3÷4 km (Friðleifsson et al., 2014). Isolating the lower part of the well
292 through proper casing – a great technological challenge per-se (Kruszewski & Wittig, 2018) – is
293 also necessary to ensure that CO_2 is injected at the proper depth.

4.3. Perspectives of technological development

295 CO_2 injectivity is controlled by reservoir permeability, which is highly dependent on temperature.
296 For example, fractured granite has a transition permeability (called elasto-plastic), which depends
297 on a threshold mean effective stress, itself a function of temperature (Watanabe et al., 2014a).
298 Above the threshold stress, permeability decreases drastically with increasing mean effective
299 stress. In contrast, fractured basalt is stable until high temperature (>500 ℃) and at 450 ℃, the
300 observed permeability depends on stress and ranges from 10^{-17} m^2 to 10^{-16} m^2 for a mean effective
301 confining stress of up to 60 MPa (Watanabe et al., 2014a). The mean effective stress in the crust
302 strongly depends on the rheology (Meyer et al., 2019; Parisio et al., 2019b) and its determination
303 at high depth and temperature remains uncertain. Considering that permeability measurements on
304 laboratory specimens tend to underestimate natural permeability at the geological scale (Neuzil,
305 1994), and that during drilling of IDDP-2, all circulation fluid was lost (Friðleifsson et al., 2017),
306 we believe that in-situ permeability ranging from 10^{-15} m^2 to 10^{-14} m^2 is possible in the fractured
307 basaltic crust (Hurwitz et al., 2007). Additionally, during injection, the fluid pressure opens up
308 pre-existing fractures, while cooling contracts the surrounding rock, generating an additional
309 fracture aperture: assuming a cubic relationship of transmissivity with fracture aperture (for which

310   fracture permeability is expressed as $k = w^2/12$, where w is the fracture aperture), an increase of

311   the fracture aperture of one order of magnitude implies an increase of the fracture transmissivity

312   of three orders of magnitude. Stimulation techniques have also the potential to achieve higher

313   permeability at depth (Watanabe et al., 2017b; 2019).

314   We estimate that suitable injection sites will permit an injection rate ranging from 0.5 to 8 Mt yr^{-}

315   ^{1} per well (Fig. 3a). Thus, for every 100 wells drilled worldwide in deep volcanic areas for

316   combined geologic carbon storage and geothermal purposes approximately 50 to 800 Mt of CO_2

317   would be stored each year without buoyancy-driven leakage risk. The number of injection wells

318   that will become operative in the next decades is highly uncertain, but to put in perspective, 100

319   wells would provide a higher amount than what is currently being stored, representing between 1

320   and 8 % of the total worldwide storage target, a non-negligible contribution to mitigate climate

321   change effects (IPPC, 2018). Our proposal is currently a blue-sky idea and several challenges need

322   to be addressed in future works, including the exact deployment of the technology, more refined

323   economical and costs/benefit analyses, pre-drilling geophysical exploration, site monitoring

324   during operation, improvements and adaptations of drilling technologies.

5. Conclusions

326   We show that storing CO_2 into reservoirs in which the resident water is in supercritical state will

327   reduce the risk of buoyancy-driven CO_2 leakage. Even when CO_2 is injected much colder than the

328   reservoir temperature, leading to CO_2 becoming locally buoyant, no buoyant forces arise around

329   the wellbore and a sinking CO_2 plume develops away from the wellbore. The injectivity per

330   wellbore is relatively high due to supercritical fluid mobility, while overpressure remains low.

331   Continuous injection of CO_2 over a decade is safe, because cooling only affects a radius in the

332   order of tens of meters from the injection wellbore. Over a longer time-span, the expansion of the

333   cooled region might increase local seismicity as faults and fractures respond to thermal induced

334   strains, limiting project lifetime. Our analyses prove that injecting into reservoirs above the critical

335   point of water would constitute a complementary solution to the problem of significantly reducing

336 CO_2 emissions and would extend the current applicability of geologic carbon storage through the

337 CO_2 sinking effect that hinders buoyancy-driven leakage to the surface.

338

Author contributions

347 F.P. and V.V. equally contributed to the design of the study, the analytical and numerical

348 computations and the writing and editing of the manuscript.

Data and materials availability

350 The calculations are easily reproducible and described in detail in the materials and methods

351 section. The FEM code for computation of CO_2 injection can be downloaded freely at

352 (https://deca.upc.edu/en/projects/code_bright). The input files for the numerical model can be

353 accessed at the institutional repository Digital.CSIC, which practices FAIR principles:

354 https://digital.csic.es/handle/10261/196740.

355 **Conflicts of interest:** There are no conflicts to declare

356

References

358 Alcalde, J., Flude, S., Wilkinson, M., Johnson, G., Edlmann, K., Bond, C.E., Scott, V., Gilfillan,

359   S.M., Ogaya, X. & Haszeldine, R.S. (2018). Estimating geological CO_2 storage security to

360   deliver on climate mitigation. *Nature Communications*, 9(1), pp.1-13.

361 Bell, I. H., Wronski, J., Quoilin, S., & Lemort, V. (2014). Pure and pseudo-pure fluid

362   thermophysical property evaluation and the open-source thermophysical property library

363   CoolProp. *Industrial & Engineering Chemistry Research, 53*(6), 2498-2508.

364 Benson, S. M., & Cole, D. R. (2008). CO_2 sequestration in deep sedimentary formations. *Elements,*
365   *4*(5), 325-331.

366 Bui, M., Adjiman, C. S., Bardow, A., Anthony, E. J., Boston, A., Brown, S., ..., & Hallett, J. P.
367   (2018). Carbon capture and storage (CCS): the way forward. *Energy & Environmental Science*,
368   *11*(5), 1062-1176.

369 Burton, M., & Bryant, S. L. (2009). Surface dissolution: minimizing groundwater impact and
370   leakage risk simultaneously. *Energy Procedia, 1*(1), 3707-3714.

371 Calcagno, P., Evanno, G., Trumpy, E., Gutiérrez-Negrín, L.C., Macías, J.L., Carrasco-Núñez, G.,
372   & Liotta, D. (2018). Preliminary 3-D geological models of los humeros and Acoculco
373   geothermal fields (Mexico)–H2020 GEMex project, *Advances in Geosciences*, *45*, 321-333.

374 Celia, M. A. (2017). Geological storage of captured carbon dioxide as a large-scale carbon
375   mitigation option. *Water Resources Research, 53*(5), 3527-3533.

376 Chiodini, G., Frondini, F., Cardellini, C., Granieri, D., Marini, L., & Ventura, G. (2001). CO_2
377   degassing and energy release at Solfatara volcano, Campi Flegrei, Italy. *Journal of Geophysical*
378   *Research: Solid Earth, 106*(B8), 16213-16221.

379 Dentz, M., & Tartakovsky, D. M. (2009). Abrupt-interface solution for carbon dioxide injection
380   into porous media. *Transport in Porous Media, 79*(1), 15-27.

381 Elders, W.A., Nielson, D., Schiffman, P., & Schriener Jr, A. (2014). Investigating ultra high-
382   enthalpy geothermal systems: a collaborative initiative to promote scientific opportunities.
383   *Scientific Drilling*, *18*(18), 35-35.

384 Friðleifsson, G. Ó., Elders, W. A., Zierenberg, R. A., Stefánsson, A., Fowler, A. P., Weisenberger,
385   T. B.., ... & Mesfin, K. G. (2017). The Iceland Deep Drilling Project 4.5 km deep well, IDDP-
386   2, in the seawater-recharged Reykjanes geothermal field in SW Iceland has successfully
387   reached its supercritical target. *Scientific Drilling, 23*, 1-12.

388 Gislason, S. R., & Oelkers, E. H. (2014). Carbon storage in basalt. *Science, 344*(6182), 373-374.

389 Goodarzi, S., Settari, A., Zoback, M. D., & Keith, D. W. (2015). Optimization of a CO_2 storage
390   project based on thermal, geomechanical and induced fracturing effects. *Journal of Petroleum*
391   *Science and Engineering, 134*, 49-59.

392 Gudmundsson, A. (2020). *Volcanotectonics: Understanding the Structure, Deformation and*
393   *Dynamics of Volcanoes*. Cambridge University Press.

394 Hitchon, B., Gunter, W. D., Gentzis, T., & Bailey, R. T. (1999). Sedimentary basins and
395   greenhouse gases: a serendipitous association. *Energy Conversion and Management, 40*(8),
396   825-843.

397 Huber, M. L., Perkins, R. A., Laesecke, A., Friend, D. G., Sengers, J.V., Assael, M. J., Metaxa, I.
398   M., Vogel, E., Mareš, R., & Miyagawa, K. (2009). New international formulation for the
399   viscosity of H_2O. *J. Phys. Chem. Ref. Data, 38*(2), 101–125.

400 Hurwitz, S., Christiansen, L. B., & Hsieh, P. A. (2007). Hydrothermal fluid flow and deformation
401   in large calderas: Inferences from numerical simulations. *Journal of Geophysical Research:*
402   *Solid Earth*, *112*(B2).

403 IPCC, (2018). Summary for Policymakers. In: Global Warming of 1.5°C. An IPCC Special Report
404   on the impacts of global warming of 1.5°C above pre-industrial levels and related global
405   greenhouse gas emission pathways, in the context of strengthening the global response to the
406   threat of climate change, sustainable development, and efforts to eradicate poverty [V. Masson-
407   Delmotte, P. Zhai, H.-O. Pörtner, D. Roberts, J. Skea, P.R. Shukla, A. Pirani, W. Moufouma-
408   Okia, C. Péan, R. Pidcock, S. Connors, J.B.R. Matthews, Y. Chen, X. Zhou, M.I. Gomis, E.
409   Lonnoy, T. Maycock, M. Tignor, and T. Waterfield (eds.)].

410 Kelemen, P. B., Matter, J. (2008). In situ carbonation of peridotite for CO_2 storage. *Proceedings*
411   *of the National Academy of Sciences*, *105*(45), 17295-17300

412 Kruszewski, M., & Wittig, V. (2018). Review of failure modes in supercritical geothermal drilling
413   projects. *Geothermal Energy, 6*(1), 28.

414 Lewicki, J. L., Birkholzer, J., & Tsang, C. F. (2007). Natural and industrial analogues for leakage
415   of CO_2 from storage reservoirs: identification of features, events, and processes and lessons
416   learned. *Environmental Geology, 52*(3), 457.

417 Lu, M., & Connell, L. D. (2014). The transient behaviour of CO_2 flow with phase transition in
418   injection wells during geological storage–Application to a case study. *Journal of Petroleum*
419   *Science and Engineering, 124*, 7-18.

420 Meyer, G.G., Brantut, N., Mitchell, T.M., & Meredith, P.G. (2019) Fault reactivation and strain
421   partitioning across the brittle-ductile transition. *Geology, 47*(12), 1127-1130.

422 Neuzil, C. E. (1994). How permeable are clays and shales?. *Water Resources Research, 30*(2),
423   145-150.

424 Nordbotten, J. M., Kavetski, D., Celia, M. A., & Bachu, S. (2008). Model for CO_2 leakage

425 including multiple geological layers and multiple leaky wells. *Environmental Science &*

426 *Technology, 43*(3), 743-749.

427 Parisio, F., Vilarrasa, V., Wang, W., Kolditz, O., & Nagel, T. (2019a). The risks of long-term re-

428 injection in supercritical geothermal systems. *Nature Communications, 10*(1), 4391.

429 Parisio, F., Vinciguerra, S., Kolditz, O., & Nagel, T. (2019b). The brittle-ductile transition in active

430 volcanoes. *Scientific Reports, 9*(1), 143.

431 Pool, M., Carrera, J., Vilarrasa, V., Silva, O., & Ayora, C. (2013). Dynamics and design of systems

432 for geological storage of dissolved CO_2. *Advances in Water Resources, 62*, 533-542.

433 Pruess, K. (2006). Enhanced geothermal systems (EGS) using CO_2 as working fluid—A novel

434 approach for generating renewable energy with simultaneous sequestration of carbon.

435 *Geothermics, 35*(4), 351-367.

436 Randolph, J. B., & Saar, M. O. (2011). Combining geothermal energy capture with geologic

437 carbon dioxide sequestration. *Geophysical Research Letters, 38*(10), GL047265.

438 Romanak, K. D., Bennett, P. C., Yang, C., & Hovorka, S. D. (2012). Process-based approach to

439 CO_2 leakage detection by vadose zone gas monitoring at geologic CO_2 storage sites.

440 *Geophysical Research Letters, 39*(15), L15405.

441 Rutqvist, J., Rinaldi, A. P., Cappa, F., Jeanne, P., Mazzoldi, A., Urpi, L., Guglielmi, Y., &

442 Vilarrasa, V. (2016). Fault activation and induced seismicity in geological carbon storage–

443 Lessons learned from recent modeling studies. *Journal of Rock Mechanics and Geotechnical*

444 *Engineering, 8*(6), 789-804.

445 Scalabrin, G., Marchi, P., Finezzo, F., & Span, R. (2006). A reference multiparameter thermal

446 conductivity equation for carbon dioxide with an optimized functional form. *J. Phys. Chem.*

447 *Ref. Data, 35*(4), 1549–1575.

448 Sigfusson, B., Gislason, S. R., Matter, J. M., Stute, M., Gunnlaugsson, E., Gunnarsson, I., ... &

449 Wolff-Boenisch, D. (2015). Solving the carbon-dioxide buoyancy challenge: The design and

450 field testing of a dissolved CO_2 injection system. *International Journal of Greenhouse Gas*

451 *Control, 37*, 213-219.

452 Span, R., & Wagner, W. (1996). A new equation of state for carbon dioxide covering the fluid

453 region from the triple point temperature to 1100 K at pressures up to 800 MPa. *J. Phys. Chem.*

454 *Ref. Data, 25*, 1509–1596.

455 Sosa-Ceballos, G., Macías, J.L., Avellán, D.R., Salazar-Hermenegildo, N., Boijseauneau-López,

456   M.E., & Pérez-Orozco, J.D. (2018). The Acoculco Caldera Complex magmas: Genesis,

457   evolution and relation with the Acoculco geothermal system. *Journal of Volcanology and*

458   *Geothermal Research*, *358*, 288-306.

459 Thiery, R., & Mercury, L. (2009). Explosive properties of water in volcanic and hydrothermal

460   systems. *Journal of Geophysical Research: Solid Earth*, *114* (B5), B05205.

461 Vilarrasa, V., Bolster, D., Dentz, M., Olivella, S., & Carrera, J. (2010). Effects of CO_2

462   compressibility on CO_2 storage in deep saline aquifers. *Transport in Porous Media, 85*(2), 619-

463   639.

464 Vilarrasa, V., Silva, O., Carrera, J., & Olivella, S. (2013). Liquid CO_2 injection for geological

465   storage in deep saline aquifers. *International Journal of Greenhouse Gas Control, 14*, 84-96.

466 Vilarrasa, V., & Carrera, J. (2015). Geologic carbon storage is unlikely to trigger large earthquakes

467   and reactivate faults through which CO_2 could leak. *Proc. Natl. Acad. Sci. U.S.A., 112*(19),

468   5938-5943.

469 Vilarrasa, V., Carrera, J., Olivella, S., Rutqvist, J., & Laloui, L. (2019). Induced seismicity in

470   geologic carbon storage. *Solid Earth, 10*(3), 871-892.

471 Wagner, W., & Pruß., A. (2002). The IAPWS Formulation 1995 for the Thermodynamic

472   Properties of Ordinary Water Substance for General and Scientific Use. *J. Phys. Chem. Ref.*

473   *Data, 31*, 387–535.

474 Watanabe, N., Numakura, T., Sakaguchi, K., Saishu, H., Okamoto, A., Ingebritsen, S.E., &

475   Tsuchiya, N. (2017a). Potentially exploitable supercritical geothermal resources in the ductile

476   crust. *Nature Geoscience, 10*(2), 140.

477 Watanabe, N., Egawa, M., Sakaguchi, K., Ishibashi, T., & Tsuchiya, N. (2017b). Hydraulic

478   fracturing and permeability enhancement in granite from subcritical/brittle to

479   supercritical/ductile conditions. *Geophysical Research Letters, 44*(11), 5468-5475.

480 Watanabe, N., Sakaguchi, K., Goto, R., Miura, T., Yamane, K., Ishibashi, T., Chen, Y., Komai,

481   T., & Tsuchiya, N. (2019). Cloud-fracture networks as a means of accessing superhot

482   geothermal energy. *Scientific Reports, 9*(1), 939.

483 Yoshioka, K., Pasikki, R., & Stimac, J. (2019). A long term hydraulic stimulation study conducted

484   at the Salak geothermal field. *Geothermics, 82*, 168-181.

Zoback, M. D., & Gorelick, S. M. (2012). Earthquake triggering and large-scale geologic storage of carbon dioxide. *Proc. Natl. Acad. Sci. U.S.A., 109*(26), 10164-10168.
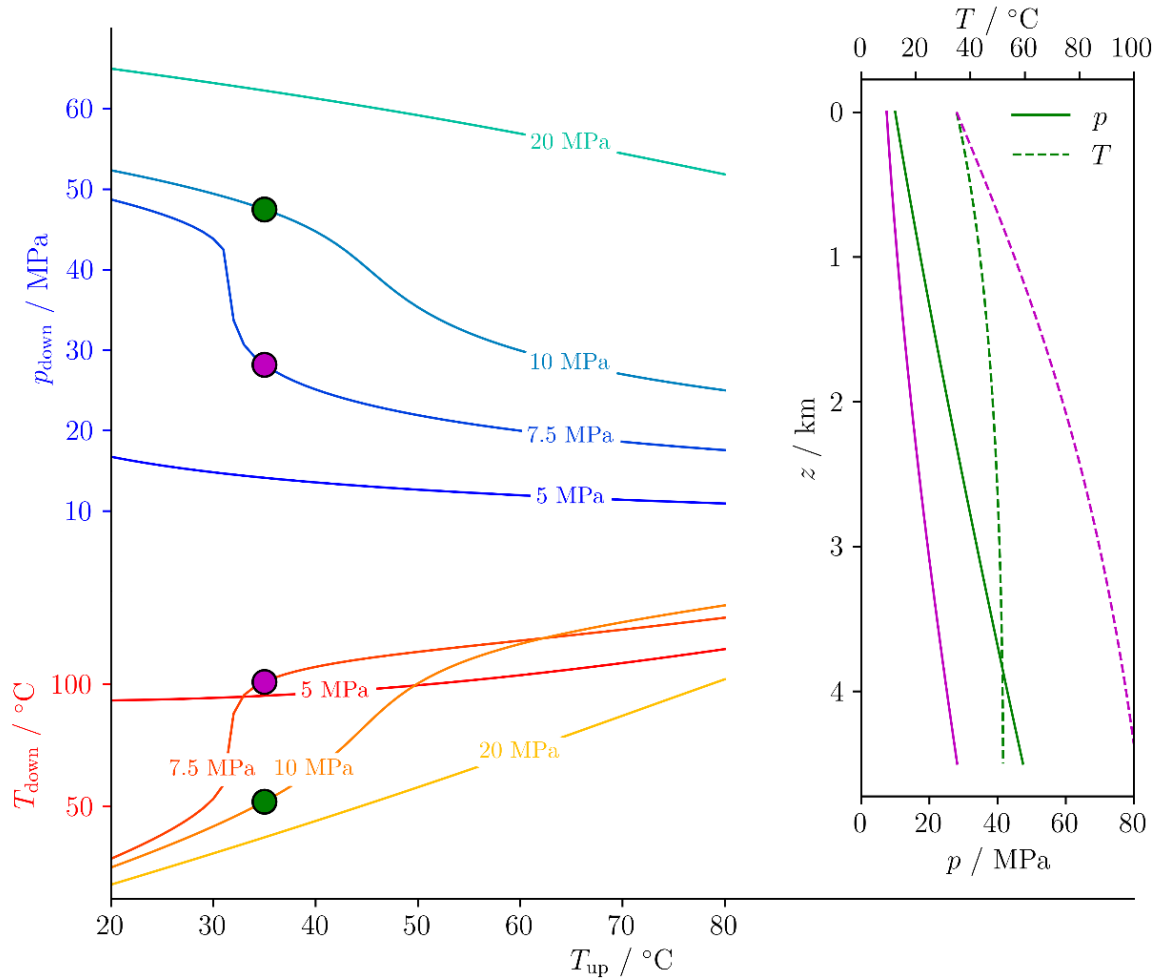
Fig. 1. CO₂ injection conditions at the wellhead and downhole. Each curve shows the pressure, p_{down}, and temperature, T_{down}, conditions at depth of injection (4.5 km) for several wellhead pressures and as a function of wellhead temperature, T_{up}. Injecting CO₂ at a higher wellhead temperature implies that it reaches the reservoir depth with a lower pressure: in order to ensure injectivity into the rock formation, a minimum downhole pressure threshold should be guaranteed and can therefore be achieved by increasing the wellhead pressure. The sharp transition in the curves corresponding to a wellhead pressure of 7.5 MPa is connected to the phase transition from liquid to supercritical close to the critical point, around which abrupt changes in density take place.

497 The inset displays the evolution of CO_2 pressure and temperature along the wellbore depth for two
498 different cases, indicated by points in the main figure (color corresponding to two different
499 wellhead conditions). Because of the adiabatic hypothesis, the heating of CO_2 is a consequence of
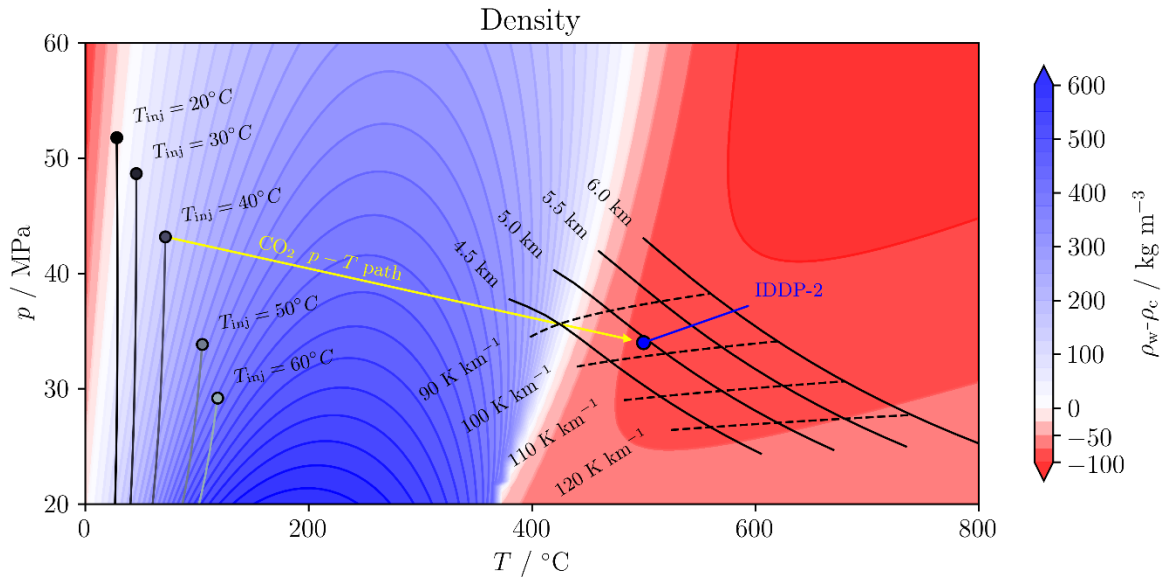500 pressure increase along the wellbore.

501

Fig. 2. Density difference map between water and CO_2. The figure shows the density difference
between water and CO_2 as a function of pressure (up to 60 MPa) and temperature (up to 800 ℃).
Positive (in blue) values indicate that CO_2 has a lower density than water, which leads to CO_2
buoyancy, and negative (in red) values indicate that CO_2 has a higher density than water, leading
to sinking potential in the reservoir. The downhole conditions of IDDP-2 are temperature of 500
℃ and pressure of 34 MPa, which would lead to CO_2 sinking potential. The dotted black lines
indicate the $p-T$ conditions of a hydrostatic water column for a variety of geothermal gradients
and the solid black lines are iso-depth for the same case. The trajectories on the left-hand side
indicate CO_2 injection conditions at the reservoir for several wellhead temperature and for a
wellhead pressure of 10 MPa. The yellow line connects the downhole conditions (buoyant) of a
hypothetical injection at IDDP2 with the CO_2 conditions (sinking) within the reservoir far from
the injection well.

514

(A) CO$_2$ plume (Dentz and Tartakovsky, 2009)

k = 10^{-14} m^2
$Q_{m,500}$ = 4.4 Mt yr^{-1}
$Q_{m,1000}$ = 8.7 Mt yr^{-1}

k = 10^{-15} m^2
$Q_{m,500}$ = 0.47 Mt yr^{-1}
$Q_{m,1000}$ = 0.95 Mt yr^{-1}

k = 10^{-17} m^2
$Q_{m,500}$ = 0.0057 Mt yr^{-1}
$Q_{m,1000}$ = 0.012 Mt yr^{-1}

k = 10^{-16} m^2
$Q_{m,500}$ = 0.054 Mt yr^{-1}
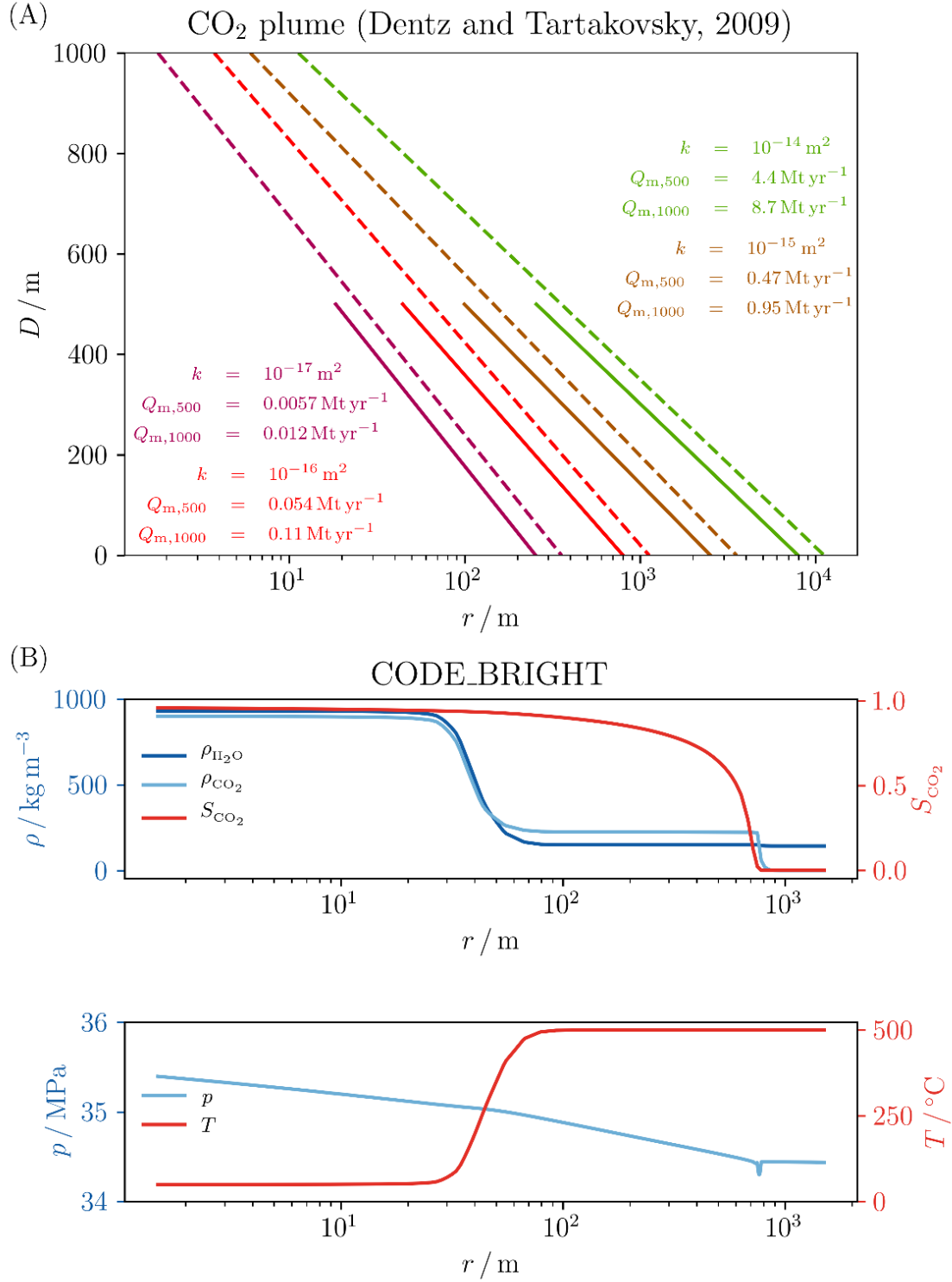$Q_{m,1000}$ = 0.11 Mt yr^{-1}

(B) CODE_BRIGHT

515

Fig. 3. CO₂ plume. (A) Analytical solutions[15,16] of the CO₂ plume position for a 10-year injection into a 500 m (solid lines) and 1000 m (dotted lines) thick reservoir. We assume a fixed

overpressure of 10 MPa at injection, isothermal injection, an initial reservoir temperature and pressure of 500 ℃ and 34 MPa, respectively, and a range of reservoir permeability, k, that spans three orders of magnitude. The mass flow rate, Q_m, is a function of the reservoir permeability and thickness. The analytical solution predicts a sinking profile due to the density difference between water and CO_2. **(B)** Simulation results after 10 years of injecting 1.0 Mt yr^{-1} of CO_2 at 50 ℃ through 500 m of open well centered into a 2000 m-thick reservoir. The extend of the cooled region has a limited size compared to the CO_2 plume and does not affect its sinking tendency.

$$\rho_{CO_2} < \rho_{H_2O} \ \& \ N \sim 10^{-1} < 1$$
$$\implies CO_2 \ \text{not floating}$$

$$N = \frac{2\pi d r_{ch} k \Delta\rho g \rho_{ch}}{\mu_{CO_2} Q_m}$$

$$\Delta\rho = \left|\rho_{CO_2} - \rho_{H_2O}\right|$$

CO₂ plume

$$\rho_{CO_2} > \rho_{H_2O} \ \& \ N \sim 10^3 \gg 1$$
$$\implies CO_2 \ \text{sinks}$$

CO₂ injection

S_{CO_2}

—— 1
—— 0.5
—— 0

H₂O

CO₂

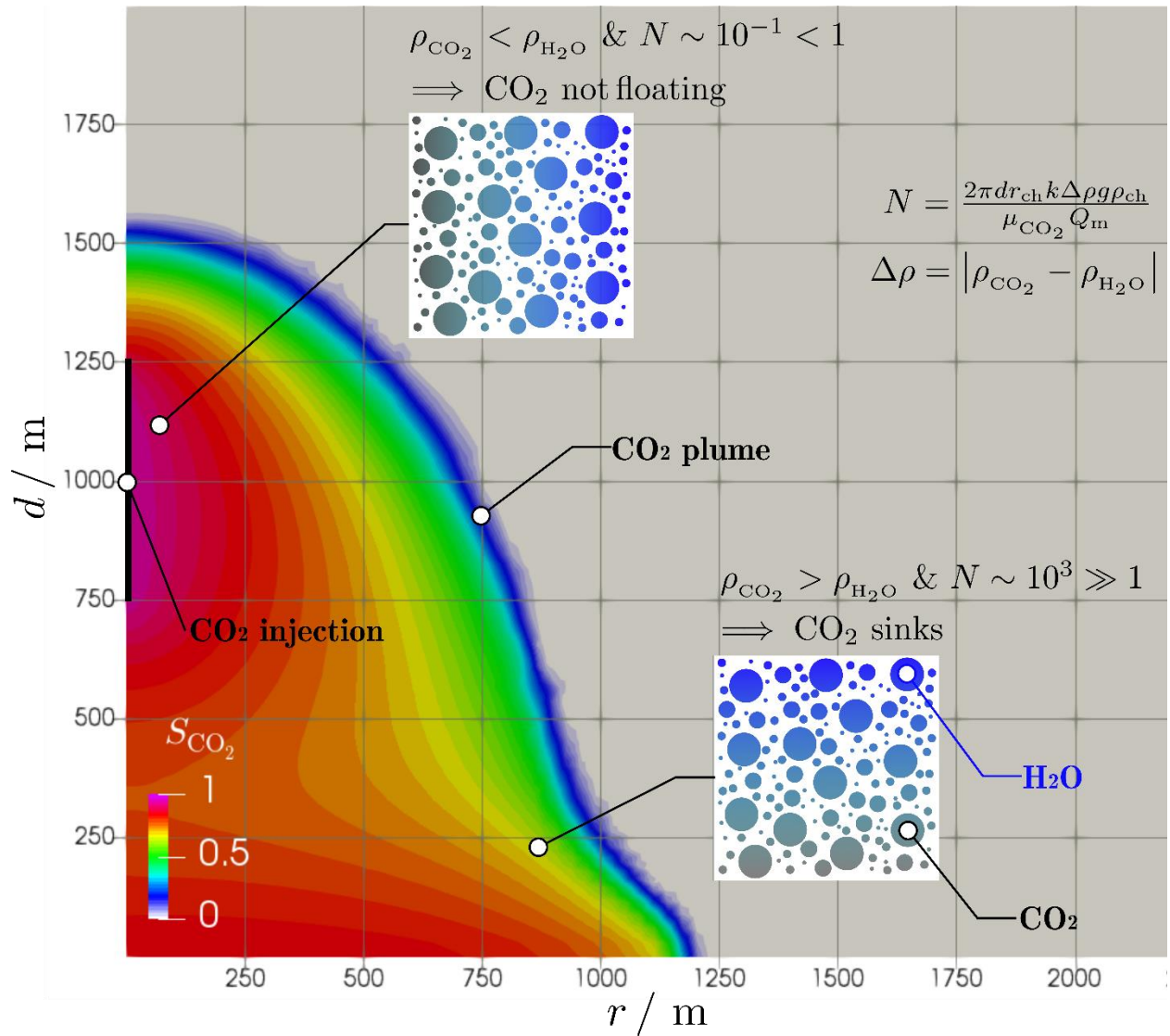$d \ / \ \text{m}$

$r \ / \ \text{m}$

528

Fig. 4. CO₂ sinking mechanism. The numerically computed sinking profile of CO₂, represented as the area with CO₂ saturation $S_c > 1$, is a consequence of the interplay between gravity and viscous forces as represented by the values of the gravity number N. Cold CO₂ injection does not increase CO₂ buoyant potential because thermal equilibrium is reached within a small region from the wellbore where viscous forces dominate over gravity forces. At the far field, CO₂ is in thermal equilibrium with the reservoir, becoming denser than water, and since gravity forces are greater than viscous ones, CO₂ has the tendency to sink.